

Iterative Learning Robust PD-SDRE Control for Active Transfemoral Prostheses

Anna Bavarsad^a, Elias August^b and Magnús Kjartan Gíslason^c
Reykjavik University, Department of Engineering, Menntavegur 1, 102 Reykjavik, Iceland

Keywords: Prosthetic Legs, Sliding Mode Control, Iterative Learning Control, SDRE, Robotics.

Abstract: In this paper, we present a novel control strategy for active prosthetic legs. The approach uses an intelligent robust Proportional-Derivative State-Dependent Riccati Equation controller to reduce the use of biomechanical energy, enhance performance and robustness. We include an Iterative Learning Control algorithm, to minimise control errors and allow the controller gains to adapt over time, and robust Sliding Mode Control to specifically address potential parametric and non-parametric uncertainties, disturbances, and noise. We conduct tests to demonstrate that the proposed controller not only maintains stability but also outperforms existing methods in terms of energy efficiency and tracking. Application of the proposed method in simulations shows significant improvements when compared to other methods from the literature, with up to 98.3% reduction in position tracking error and up to 91.9% reduction in control cost. Furthermore, for angular tracking of the hip and knee, improvements of up to 32.6% and 44.9%, along with torque reductions of up to 67.5% and 87.5%, are observed. This study represents a step forward in providing an effective solution for controlling active prosthetic devices.

1 INTRODUCTION

The global incidence of lower limb amputation continues to rise, with over 200,000 cases reported annually in the United States alone (McDonald et al., 2021, Ziegler-Graham et al., 2008), while there is an urgent need for advanced prosthetic solutions that restore natural gait and improve the overall quality of life for amputees. Amputations can occur at various levels, including transtibial (below the knee), transfemoral (above the knee), foot amputations, and hip and knee disarticulations (Kibria and Commuri, 2024). Restoring complete mobility remains particularly challenging for transfemoral amputees. Currently, there are three primary types of prosthetic legs: passive, active (with motor control), and semi-active ones (control without motors). Passive prostheses require users to engage their residual hip joint to move the prosthetic knee, which leads to increased effort, of up to 60% more biomechanical energy usage compared to other individuals, and potential discomfort (Bukowski, 2006 and Chin et al.,

2005). Active prostheses offer some key advantages over passive ones, such as a reduced energy usage, improved stability, and more natural movement (Orendurff et al., 2006, Kaufman et al., 2008, Camargo et al., 2022). However, they require complex control systems and are more expensive. Moreover, ensuring stability, responsiveness, and energy efficiency is challenging in the presence of uncertainties and disturbances (Müßig et al., 2019, Martini et al., 2020). Users of robotic leg prostheses often struggle with stability and symmetry compared to healthy individuals, largely due to system uncertainties and environmental disturbances, such as unknown mass distribution and complex foot-ground interactions, respectively, and sensor noise (Ma et al., 2024).

Designing controllers that provide performance for different users and environments remains challenging (Kashiri et al., 2018). In this paper, we propose a novel control strategy to address the following multiple control objectives simultaneously: energy efficiency, accurate trajectory tracking, and

^a  <https://orcid.org/0000-0002-6444-487X>

^b  <https://orcid.org/0000-0001-9018-5624>

^c  <https://orcid.org/0000-0003-0872-5201>

robustness. While recent studies, such as (Saat et al., 2024), have explored various advancements in Proportional-Integral-Derivative (PID) and Proportional-Derivative (PD) control methods, this work focuses on a novel approach by proposing an intelligent PD State-Dependent Riccati Equation (PD-SDRE) control approach, which merges the effectiveness of a traditional PD controller with the advanced optimisation capabilities of SDRE control. SDRE control is designed for systems whose dynamics explicitly depend on the state. It aims to minimise a predefined cost function while maintaining stability. SDRE control does not require model linearisation, but the dynamic adjustment of controller gains based on the system's state, making it particularly effective for complex nonlinear systems (Çimen, 2008, Nekoo, 2019). It has been successfully applied in various fields, especially robotics (Bavarsad et al., 2020, Bavarsad et al., 2021).

To further improve the controller, we also integrate an Iterative Learning Control (ILC) algorithm. ILC is particularly useful in environments that call for repeated tasks, as it progressively optimises the control using data from prior iterations. This allows the system to "learn" from previous errors and to improve the performance. Given the repetitive nature of activities such as walking and climbing stairs, ILC is particularly suitable for improving performance over time after the PD-SDRE controller provides the initial input (Ahn et al., 2007, Shen, 2018, Nekoo et al., 2022, Memon and Shao, 2021).

Our approach also includes the integration of robust Sliding Mode Control (SMC) for managing uncertainties. In principle, it drives the system's state to "slide" along a predefined surface, known as the sliding surface, on which the system exhibits simplified behaviour. Once on this surface, the dynamics of the system become less sensitive to model uncertainties and external disturbances, making SMC particularly useful in unpredictable environments (Slotine and Li, 1991). This paper introduces the following key innovations:

1. Application of PD-SDRE with ILC: To our knowledge, this study is the first one to apply PD-SDRE in combination with ILC to active prosthetic legs.
2. Enhanced Robustness through SMC: Our integration of robust SMC techniques improves the system's ability to cope with parametric and non-parametric uncertainties while maintaining stability and performance.
3. Simplified Desired Dynamics Calculation in ILC: We simplify the dynamics calculations required by the ILC. Instead of computing the Jacobian

matrix, we use desired trajectory values for position, velocity, and acceleration for the calculation of the desired dynamics. This reduces computational complexity and broadens the controller's applicability to various robotic systems, including active prosthetic legs. Simulations show that this modified ILC approach effectively learns desired dynamics to improve trajectory tracking over time.

The structure of the remainder of this paper is the following. In Section 2, we present the model for an active transfemoral prosthesis and in Section 3, the design of the ILC robust PD-SDRE controller. Section 4 provides simulation results and shows the effectiveness of our approach. Section 5 discusses the results and concludes the paper.

2 DYNAMIC MODEL OF AN ACTIVE TRANSFEMORAL PROSTHESIS

The three degrees-of-freedom dynamical model for the active transfemoral prosthesis is given by (Azimi et al., 2015):

$$\begin{aligned} & \left(\mathbf{M}_P(\mathbf{q}(t)) \right) \ddot{\mathbf{q}}(t) + \left(\mathbf{C}_P(\mathbf{q}(t), \dot{\mathbf{q}}(t)) \right) \dot{\mathbf{q}}(t) \\ & + \mathbf{G}_P(\mathbf{q}(t)) + \mathbf{R}_P(\mathbf{q}(t), \dot{\mathbf{q}}(t)) \\ & = \mathbf{u}(t) - \mathbf{T}_e(\mathbf{q}(t)). \end{aligned} \quad (1)$$

In (1), $\mathbf{M}_P(\mathbf{q}(t))$ is the invertible inertia matrix, $\mathbf{C}_P(\mathbf{q}(t), \dot{\mathbf{q}}(t))$ represents the Coriolis and centripetal matrix, $\mathbf{G}_P(\mathbf{q}(t))$ denotes the gravity vector, and $\mathbf{R}_P(\mathbf{q}(t), \dot{\mathbf{q}}(t))$ accounts for the nonlinear damping vector. Vector $\mathbf{q}^T = [q_1 \ q_2 \ q_3]$ describes the displacement of the joints, where q_1 corresponds to the hip vertical displacement, q_2 is the thigh angle, and q_3 is the knee angle. $\mathbf{u}(t)$ includes the control force at the hip and the control torques at thigh and knee joints. Term $\mathbf{T}_e(\mathbf{q}(t))$ captures the combined effects of the horizontal, F_x , and the vertical, F_z , components of the ground reaction force (GRF) on each joint. The complete equations are:

$$\begin{aligned} P_1 &= m_1 + m_2 + m_3, \\ P_2 &= m_3 l_2 + m_2 l_2 + m_2 c_2, \quad P_3 = m_3 c_3, \\ P_4 &= I_{2z} + I_{3z} + m_2 c_2^2 + m_3 c_2^2 + m_2 l_2^2 + m_3 l_2^2 + \\ & \quad 2m_2 c_2 l_2, \\ P_5 &= m_3 c_3 l_2, \quad P_6 = m_3 c_3^2 + I_{3z}, \quad P_7 = b, \quad P_8 = f, \end{aligned}$$

$$\mathbf{M}_P = \begin{bmatrix} P_1 & m_p & P_3 \cos(q_2 + q_3) \\ m_p & P_4 + 2P_5 \cos q_3 & P_6 + P_5 \cos q_3 \\ P_3 \cos(q_2 + q_3) & P_6 + P_5 \cos q_3 & P_6 \\ m_p = P_3 \cos(q_2 + q_3) + P_2 \cos q_2, & & \end{bmatrix}$$

$$\mathbf{C}_P = \begin{bmatrix} 0 & c_{P1} - \dot{q}_2 P_2 \sin q_2 & c_{P1} \\ 0 & -\dot{q}_3 P_5 \sin q_3 & c_{P2} \\ 0 & \dot{q}_2 P_5 \sin q_3 & 0 \end{bmatrix}, \quad (2)$$

$$c_{P1} = -\dot{q}_2 P_3 \sin(q_2 + q_3) - \dot{q}_3 P_3 \sin(q_2 + q_3),$$

$$c_{P2} = -\dot{q}_2 P_5 \sin q_3 - \dot{q}_3 P_5 \sin q_3,$$

$$\mathbf{G}_P = -g \begin{bmatrix} P_1 \\ P_2 m_P \\ P_3 \cos(q_2 + q_3) \end{bmatrix}, \quad \mathbf{R}_P = \begin{bmatrix} P_8 \tanh \dot{q}_1 \\ P_7 \dot{q}_2 \\ 0 \end{bmatrix},$$

$$\mathbf{T}_e(\mathbf{q}(t)) = \begin{bmatrix} F_Z \\ F_Z(l_2 \cos q_2 + l_3 c_{23}) - F_X(l_2 \sin q_2 + l_3 s_{23}) \\ F_Z(l_3 c_{23}) - F_X(l_3 s_{23}) \end{bmatrix},$$

$$c_{23} = \cos(q_2 + q_3), \quad s_{23} = \sin(q_2 + q_3)$$

$$L_z = q_1 + l_2 \sin q_2 + l_3 s_{23},$$

$$F_Z = \begin{cases} 0 & , L_z < S_z \\ k_b |S_z - L_z| & , L_z > S_z \end{cases}, \quad F_X = \beta F_Z.$$

As in (Azimi et al., 2015), we assume that a treadmill is used as walking surface and the treadmill belt is modelled by a mechanical spring. In (2), L_z represents the vertical position of the lower leg in the belt's global coordinate system (x_0, y_0, z_0) (see Figure 1). Description and specific nominal values for the model and the treadmill parameters are provided in Table 1.

To allow for a comparison with the results in (Bavarsad et al., 2020) and (Azimi et al., 2015), we use parameters from these references. State vector, input vector, and reference trajectory are

$$\begin{aligned} \mathbf{x}^T(t) &= [q_1 \quad q_2 \quad q_3 \quad \dot{q}_1 \quad \dot{q}_2 \quad \dot{q}_3], \\ \mathbf{u}^T(t) &= [F_{Hip} \quad \tau_{Thigh} \quad \tau_{Knee}], \\ \mathbf{r}^T(t) &= [r_1 \quad r_2 \quad r_3 \quad \dot{r}_1 \quad \dot{r}_2 \quad \dot{r}_3 \quad \ddot{r}_1 \quad \ddot{r}_2 \quad \ddot{r}_3]. \end{aligned} \quad (3)$$

For $\mathbf{r}(t)$, we use walking data from the Motion Study Laboratory at the Cleveland Department of Veterans Affairs Medical Center (Azimi et al., 2015). Finally, the state-space representation of system (1) is given by

$$\begin{bmatrix} \dot{x}_1 \\ \dot{x}_2 \\ \dot{x}_3 \\ \dot{x}_4 \\ \dot{x}_5 \\ \dot{x}_6 \end{bmatrix} = \begin{bmatrix} x_4 \\ x_5 \\ x_6 \\ v_1 \\ v_2 \\ v_3 \end{bmatrix}, \quad (4)$$

$$\mathbf{v}(t) = \mathbf{M}_P^{-1}(\mathbf{u}(t) - \mathbf{T}_e - \mathbf{C}_P \dot{\mathbf{q}} - \mathbf{G}_P - \mathbf{R}_P).$$

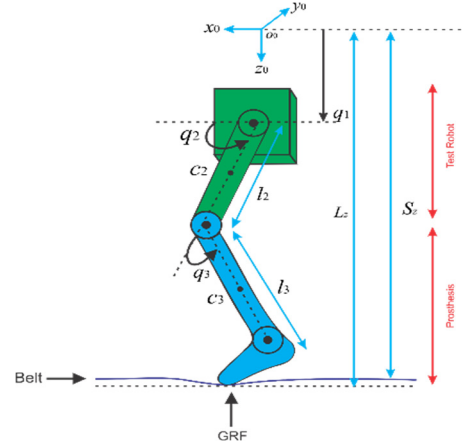


Figure 1: The Prismatic-Revolute-Revolute structure of the active transfemoral prosthesis (Azimi et al., 2015).

Table 1: Nominal values and specific parameters for prosthesis model and treadmill.

Description	Parameter	Nominal value	Unit
Mass of link 1	m_1	40.5969	kg
Mass of link 2	m_2	8.5731	kg
Mass of link 3	m_3	2.29	kg
Thigh length	l_2	0.425	m
Length from knee joint to bottom of shoe	l_3	0.527	m
Center of mass on thigh	c_2	0.09	m
Center of mass on shank	c_3	0.32	m
Rotary inertia of link 2	I_{2z}	0.138	kgm ²
Rotary inertia of link 3	I_{3z}	0.0618	kgm ²
Sliding friction in link 1	f	83.33	N
Rotary actuator damping	b	9.75	Nms
Acceleration of gravity	g	9.81	m/s ²
Vertical distance from the origin of belt frame	S_z	0.905	m
Belt stiffness	K_b	37000	N/m
Friction coefficient	β	0.2	-

3 LEARNING CONTROL WITH ROBUST PD - SDRE

3.1 SDRE

Consider the following uncertain nonlinear system,

$$\dot{\mathbf{x}}(t) = \hat{\mathbf{f}}(\mathbf{x}(t)) + \hat{\mathbf{g}}(\mathbf{x}(t))\mathbf{u}(t). \quad (5)$$

In (5), $\hat{\mathbf{f}}(\mathbf{x}(t))$ and $\hat{\mathbf{g}}(\mathbf{x}(t))\mathbf{u}(t)$ represent the actual system dynamics, which include uncertainties due to unknown but bounded parameter values. Next, we transform (5) using State Dependent Coefficients parametrisation matrices, that is, we let $\mathbf{f}(\mathbf{x}(t)) =$

$A(\mathbf{x}(t))\mathbf{x}(t)$, $A(\mathbf{x}(t)): \mathbb{R}^n \rightarrow \mathbb{R}^{n \times n}$, and $\mathbf{g}(\mathbf{x}(t)) = \mathbf{B}(\mathbf{x}(t))$, $\mathbf{B}(\mathbf{x}(t)): \mathbb{R}^n \rightarrow \mathbb{R}^{n \times m}$, and consider the following nonlinear dynamical system,

$$\begin{aligned} \dot{\mathbf{x}}(t) &= \mathbf{A}(\mathbf{x}(t))\mathbf{x}(t) + \mathbf{B}(\mathbf{x}(t))\mathbf{u}(t), \\ \mathbf{y}(t) &= \mathbf{C}(\mathbf{x}(t))\mathbf{x}(t). \end{aligned} \quad (6)$$

Note that matrices $\mathbf{A}(\mathbf{x}(t))$ and $\mathbf{B}(\mathbf{x}(t))$ are not unique (Çimen, 2008). In this paper,

$$\begin{aligned} \mathbf{A}(\mathbf{x}(t))_{6 \times 6} &= \begin{bmatrix} 0_{3 \times 3} & I_{3 \times 3} \\ 0_{3 \times 3} & -\mathbf{M}_{P_{3 \times 3}}^{-1}(\mathbf{x}(t))\mathbf{C}_{P_{3 \times 3}}(\mathbf{x}(t), \dot{\mathbf{x}}(t)) \end{bmatrix}, \\ \mathbf{B}(\mathbf{x}(t))_{6 \times 3} &= \begin{bmatrix} 0_{3 \times 3} \\ \mathbf{M}_{P_{3 \times 3}}^{-1}(\mathbf{x}(t)) \end{bmatrix}, \\ \mathbf{C}(\mathbf{x}(t))_{6 \times 6} &= I_{6 \times 6}. \end{aligned} \quad (7)$$

Definition 1 (Çimen, 2008): (6) is stabilisable (controllable) if, for every $\mathbf{x} \in \Omega$, the pair $\{\mathbf{A}(\mathbf{x}(t)), \mathbf{B}(\mathbf{x}(t))\}$ is pointwise linear stabilisable (controllable).

Definition 2 (Çimen, 2008): (6) is detectable (observable) if, for every $\mathbf{x} \in \Omega$, the pair $\{\mathbf{A}(\mathbf{x}(t)), \mathbf{C}(\mathbf{x}(t))\}$ is pointwise linear detectable (observable).

If (6) is controllable and observable, then an optimal controller is obtained by minimising cost function

$$J_0 = \frac{1}{2} \int_0^{\infty} (\mathbf{x}^T(t)\mathbf{C}^T\mathbf{Q}\mathbf{C}\mathbf{x}(t) + \mathbf{u}^T(t)\mathbf{R}\mathbf{u}(t))dt, \quad (8)$$

where weighting matrices \mathbf{Q} and \mathbf{R} are positive definite. The optimal control law is then given by

$$\mathbf{u}_{(SDRE)}(t) = -\mathbf{R}^{-1}\mathbf{B}^T(\mathbf{x})\mathbf{K}(\mathbf{x})[\mathbf{e}, \dot{\mathbf{e}}]^T, \quad (9)$$

where $\mathbf{e} = \mathbf{x} - \mathbf{r}$, $\dot{\mathbf{e}} = \dot{\mathbf{x}} - \dot{\mathbf{r}}$, and matrix $\mathbf{K}(\mathbf{x}(t))$ is determined by solving the following algebraic SDRE:

$$\begin{aligned} \mathbf{A}^T(\mathbf{x})\mathbf{K}(\mathbf{x}) + \mathbf{K}(\mathbf{x})\mathbf{A}(\mathbf{x}) - \\ \mathbf{K}(\mathbf{x})\mathbf{B}(\mathbf{x})\mathbf{R}^{-1}\mathbf{B}^T(\mathbf{x})\mathbf{K}(\mathbf{x}) + \mathbf{C}^T\mathbf{Q}\mathbf{C} = \mathbf{0}. \end{aligned} \quad (10)$$

Note also that we will partition $\mathbf{K}(\mathbf{x})$ into the following four-square blocks:

$$\mathbf{K}(\mathbf{x}) = \begin{bmatrix} \mathbf{K}_{11}(\mathbf{x}) & \mathbf{K}_{12}(\mathbf{x}) \\ \mathbf{K}_{12}^T(\mathbf{x}) & \mathbf{K}_{22}(\mathbf{x}) \end{bmatrix}. \quad (11)$$

Finally, as in (Nekoo, 2019, Bavarsad et al., 2021), we incorporate unfactored terms into

$$\mathbf{u}_{add}(t) = \mathbf{G}_p(\mathbf{q}(t)) + \mathbf{R}_p(\mathbf{q}(t)) + \mathbf{T}_e(\mathbf{q}(t)) \quad (12)$$

such that the control law becomes

$$\mathbf{u}(t) = \mathbf{u}_{(SDRE)}(t) + \mathbf{u}_{add}(t). \quad (13)$$

3.2 PD - SDRE

To include PD control, the control law is modified to:

$$\mathbf{u}_{(PD-SDRE)}(t) = -\mathfrak{N}_1(\mathbf{x})\mathbf{e} - \mathfrak{N}_2(\mathbf{x})\dot{\mathbf{e}}, \quad (14)$$

$$\mathfrak{N}_1(\mathbf{x}) = \mathbf{R}^{-1}\mathbf{M}_P^{-1}\mathbf{K}_{12}^T, \quad (15)$$

$$\mathfrak{N}_2(\mathbf{x}) = \mathbf{R}^{-1}\mathbf{M}_P^{-1}\mathbf{K}_{22}. \quad (16)$$

Note that matrices (15) and (16) are not necessarily symmetric positive definite. To ensure the stability of the controller, the gain matrices must be symmetric positive definite (Nekoo et al., 2022). To address this, we consider the following transformation,

$$\mathbf{K}_{SP}(\mathbf{x}) = \frac{\mathbf{K}_{12}\mathbf{M}_P^{-1}\mathbf{R}^{-1}\mathbf{M}_P^{-1}\mathbf{K}_{12}^T}{\|\mathbf{K}_{12}\mathbf{M}_P^{-1}\|_2}, \quad (17)$$

$$\mathbf{K}_{SD}(\mathbf{x}) = \frac{\mathbf{K}_{22}^T\mathbf{M}_P^{-1}\mathbf{R}^{-1}\mathbf{M}_P^{-1}\mathbf{K}_{22}}{\|\mathbf{K}_{22}\mathbf{M}_P^{-1}\|_2}, \quad (18)$$

and reformulate control law (14) such that

$$\mathbf{u}_{(PD-SDRE)}(t) = -\mathbf{K}_{SP}(\mathbf{x})\mathbf{e} - \mathbf{K}_{SD}(\mathbf{x})\dot{\mathbf{e}}. \quad (19)$$

As proving stability for this control law follows a procedure like the one in (Nekoo et al., 2022), the details are omitted.

3.3 Robust SMC PD - SDRE

For robustness, we follow the approach presented in (Slotine and Li, 1991) and define the following first order sliding surface,

$$\mathbf{s}(\mathbf{x}, t) = \dot{\mathbf{e}}(\mathbf{x}, t) + \mathbf{\Gamma}\mathbf{e}(\mathbf{x}, t), \quad (20)$$

where $\mathbf{\Gamma}$ is a strictly positive constant matrix, determined by the user. To drive the system towards the sliding surface $\mathbf{s} = \mathbf{0}$, we add the following to the control,

$$\mathbf{u}_{SMC}(t) = -\mathbf{K}_d \mathbf{s} \mathbf{gn}(\mathbf{s}), \quad (21)$$

where $\mathbf{K}_d = \text{diag}(k_{d_1}, k_{d_2}, k_{d_3})$ is a strictly positive constant matrix. Since SMC suffers from the chattering phenomenon, which arises from the discontinuous nature of the sign function, we replace $\mathbf{sgn}(s_i)$ by saturation function $\text{sat}(s_i/\varphi_i)$, where $\text{sat}(s_i/\varphi_i) = s_i/\varphi_i$ if $|s_i/\varphi_i| < 1$, $\text{sat}(s_i/\varphi_i) = \mathbf{sgn}(s_i)$ otherwise, and $\varphi_i > 0$ (Slotine and Li, 1991). The control law is now given by

$$\begin{aligned} \mathbf{u}_{Robust-PD-SDRE}(t) &= \mathbf{u}_{PD-SDRE} + \mathbf{u}_{SMC} = \\ &= -\mathbf{K}_{SP}(\mathbf{x})\mathbf{e} - \mathbf{K}_{SD}(\mathbf{x})\dot{\mathbf{e}} - \mathbf{K}_d \text{sat}(\Phi^{-1}\mathbf{s}), \Phi_{i,i} = \\ \varphi_i, \Phi_{i,j \neq i} &= 0. \end{aligned} \quad (22)$$

3.4 Iterative Learning Robust PD -SDRE Control

To apply ILC, we modify the equation of motion by adding and subtracting desired dynamics ($\mathbf{D}_d(\ddot{\mathbf{r}}, \dot{\mathbf{r}}, \mathbf{r})$) from (1):

$$\begin{aligned} &[\mathbf{M}_P(\mathbf{q}) - \mathbf{M}_P(\mathbf{r})](\ddot{\mathbf{q}} - \ddot{\mathbf{r}}) + [\mathbf{C}_P(\mathbf{q}, \dot{\mathbf{q}}) - \\ &\mathbf{C}_P(\mathbf{r}, \dot{\mathbf{r}})](\dot{\mathbf{q}} - \dot{\mathbf{r}}) + \mathbf{G}_P(\mathbf{q}) + \mathbf{R}_P(\mathbf{q}, \dot{\mathbf{q}}) + \mathbf{T}_e = \\ &\mathbf{u}(t) - \mathbf{D}_d(\ddot{\mathbf{r}}, \dot{\mathbf{r}}, \mathbf{r}), \end{aligned} \quad (23)$$

Where

$$\mathbf{D}_d(\ddot{\mathbf{r}}, \dot{\mathbf{r}}, \mathbf{r}) = \mathbf{M}_P(\mathbf{r})\ddot{\mathbf{r}} + \mathbf{C}_P(\mathbf{r}, \dot{\mathbf{r}})\dot{\mathbf{r}}. \quad (24)$$

Since we wish to minimise the sum of tracking errors over time, the performance index is defined as follows,

$$J_{IT} = \frac{1}{2} \sum_{i=1}^{N_i} \|\mathbf{H}_{ILC}^i(t) - \mathbf{D}_d^i(t)\|^2, \quad (25)$$

where N_i is the number of iterations and $\mathbf{D}_d^i(t)$ is the desired dynamics at the i -th iteration. We, thus, express the final control law as

$$\mathbf{u}_{Final}(t) = \mathbf{u}_{Robust-PD-SDRE}(t) + \mathbf{H}_{ILC}^i(t) + \mathbf{u}_{add}(t). \quad (26)$$

Applying the gradient descent method to (25) yields the following training rule updating $\mathbf{H}_{ILC}^i(t)$:

$$\begin{aligned} \mathbf{H}_{ILC}^i &= \mathbf{H}_{ILC}^{i-1} - \alpha \times (\mathbf{H}_{ILC}^{i-1} - \mathbf{D}_d^{i-1}(t)), \\ 0 < \alpha < 1. \end{aligned} \quad (27)$$

Training rule (27) uses the desired dynamics to update the control, where learning rate α is a constant scalar (Nekoo et al., 2022).

Note that this paper presents an alternative approach to (Nekoo et al., 2022). In (Nekoo et al., 2022), computing the desired dynamics requires, both, the forward kinematics and the Jacobian matrix. However, for some systems, the determinant of the Jacobian matrix can become zero (see (Richter and Simon, 2015)), which renders the approach unsuitable for them. We circumvent the need for above computations by using directly the desired trajectory values for position, velocity, and acceleration, given in (24). Figure 2 provides a block diagram that illustrates the overall system architecture and highlights the integration and interaction among the components of the proposed three-layer control framework.

4 SIMULATION RESULTS

DC motors are responsible for generating the torque necessary for operating the prosthesis. These motors have specific speed and torque limitations, which determine permissible control signal ranges, and are given by:

$$u_i(t) = \begin{cases} u_{i,max}(t) & \text{if } u_i(t) > u_{i,max}(t) \\ u_i(t) & \text{if } u_{i,min}(t) < u_i(t) < u_{i,max}(t) \\ u_{i,min}(t) & \text{if } u_{i,min}(t) > u_i(t), i = 1,2,3. \end{cases} \quad (28)$$

To closely align simulation results with reality, we use the following saturation limits: (−1200 N, 1200 N) for hip displacement force, (−900 Nm, 900 Nm) for thigh torque, and (−400 Nm, 400 Nm) for knee torque.

To assess the performance of the proposed control, we employ two metrics: The Root Mean Square Error, $RMSE_i$, for each state and the Root Mean Square for each control input $RMSU_j$. These metrics evaluate the steady-state error and control effort, providing a measure of controller performance:

$$RMSE_i = \sqrt{\frac{1}{T} \int_0^T (x_i - r_i)^2 dt}, \quad i = 1,2,3, \quad (29)$$

$$RMSU_j = \sqrt{\frac{1}{T} \int_0^T (u_j)^2 dt}, \quad j = 1,2,3$$

For comparing the proposed method with those in references (Bavarsad et al., 2020) and (Azimi et al., 2015), we use the same initial conditions. Specifically, the initial state is set to $\mathbf{x}_{initial} = [0.019, 1.13, 0.09, 0.09, 0, 1.6]^T$ (omitting units). Weighting matrices \mathbf{Q} and \mathbf{R} , along with the design parameters for the ILC and SMC, represented by \mathbf{K}_d , $\mathbf{\Gamma}$, and Φ , are specified in Table 2.

Table 2: Controllers' parameters.

Controllers	Design Parameters and Values
PD-SDRE	$\mathbf{Q} = \text{diag}[10^{13}, 10^{11}, 10^{11}, 10^6, 10^5, 5 \times 10^5]$
	$\mathbf{R} = \text{diag}[0.1, 0.1, 0.1]$
ILC	$\alpha = 0.7$
	Number of iterations = 10
SMC	$\mathbf{K}_d = \text{diag}[50, 75, 40]$
	$\mathbf{\Gamma} = \text{diag}[51, 27, 9]$
	$\Phi = \text{diag}[2, 2, 2]$

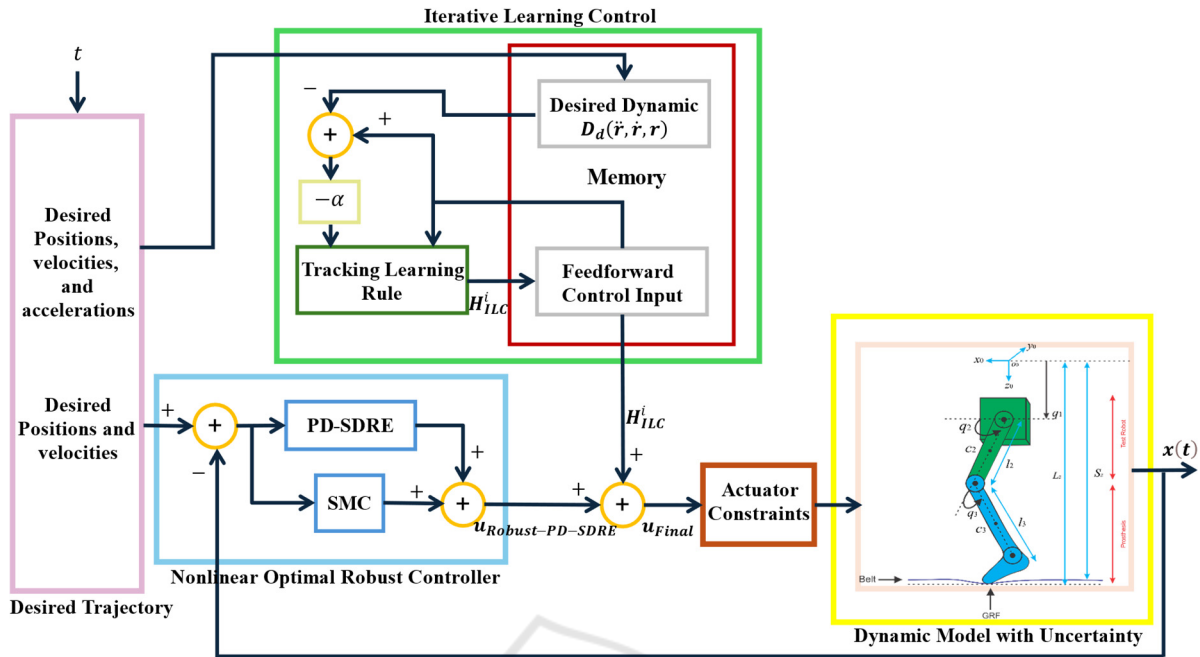


Figure 2: A control system block diagram of proposed approach.

4.1 Nominal Parameter Values

Table 3 provides a detailed comparison of the RMSE and the RMSU, where, for better comparability, we “normalised” $RMSE_1$ by dividing it by 0.02 m (maximal hip displacement). The results show significant improvements in, both, tracking accuracy and energy efficiency of the proposed control approach (ILC + PD-SDRE + SMC) relative to two other methods: Integral State Control + SDRE + SMC (Bavarsad et al., 2020) and Robust Adaptive Impedance Control (Azimi et al., 2015). In position tracking ($RMSE_1$), our method reduces the error by 95.4% relative to (Bavarsad et al., 2020) and by 98.3% relative to (Azimi et al., 2015). For the first angular tracking metric $RMSE_2$, an improvement of 32.6% compared to (Bavarsad et al., 2020) and 28.1% compared to (Azimi et al., 2015) is achieved, while the second angular tracking metric $RMSE_3$ shows a 44.9% improvement over (Azimi et al., 2015).

In terms of control cost, the proposed strategy achieves reductions of 77.8% and 91.9% compared to (Bavarsad et al., 2020) and (Azimi et al., 2015) in $RMSU_1$, respectively. The first control torque metric $RMSU_2$ indicates a 67.5% improvement over (Azimi et al., 2015) but a 35.8% increase over (Bavarsad et al., 2020). For the second control torque metric $RMSU_3$, we observe reductions of 87.5% relative to (Azimi et al., 2015) and an increase of 75.8% compared to (Bavarsad et al., 2020). While the

proposed approach improves tracking performance and energy efficiency, we see that they may not improve simultaneously.

The integration of ILC leads to improvements in various performance parameters. Notably, the displacement error improves by 2.36%, while the first angular parameter shows an 8.13% reduction in error and the second angular parameter improves by 4.77%. Furthermore, the necessary force is reduced by 0.72% and the torque by 12.42%. However, there is a slight increase in knee torque of 3.59%.

Table 3: Comparison with references (Bavarsad et al., 2020), (Azimi et al., 2015).

	ILC + PD-SDRE + SMC	PD-SDRE + SMC	Integral State Control + SDRE + SMC (Bavarsad et al., 2020)	Robust Adaptive Impedance Control (Azimi et al., 2015)
$\frac{RMSE_1}{0.02 \text{ m}}$	0.0120	0.0123	0.26	0.715
$RMSE_2$ (rad)	0.0032	0.0035	0.0048	0.0045
$RMSE_3$ (rad)	0.0030	0.0031	0.0011	0.0054
$RMSU_1$ (N)	31.6	31.8	142	388
$RMSU_2$ (Nm)	22.1	25.23	16.28	68
$RMSU_3$ (Nm)	4.514	4.358	2.568	36

4.2 Changing Parameter Values

To test the robustness of the proposed approach, first, we investigate the effect of a $\pm 30\%$ change in the parameters' vector. We observe a minor increase/decrease in tracking error and control cost. Figure 3 illustrates the horizontal and vertical GRFs. The resulting forces closely match those observed in able-bodied individuals. Figure 4 depicts the performance of the proposed controller in tracking desired trajectories. Despite non-zero initial errors in all states, the controlled system quickly converges to desired values. Moreover, despite a $\pm 30\%$ change in system parameters, the amplitudes in the graphs exhibit very minimal variations. This indicates the reliability of the proposed method.

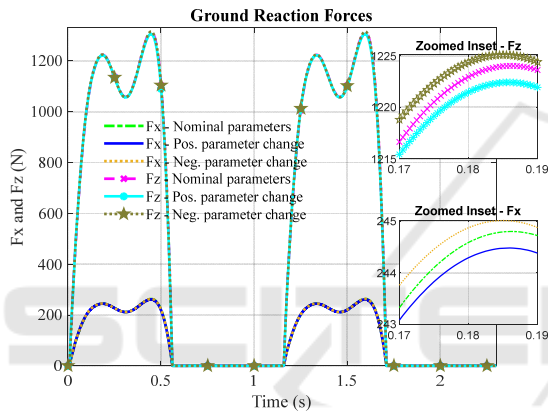


Figure 3: Horizontal and vertical GRF in nominal mode and $\pm 30\%$ parametric change, considering saturation bounds.

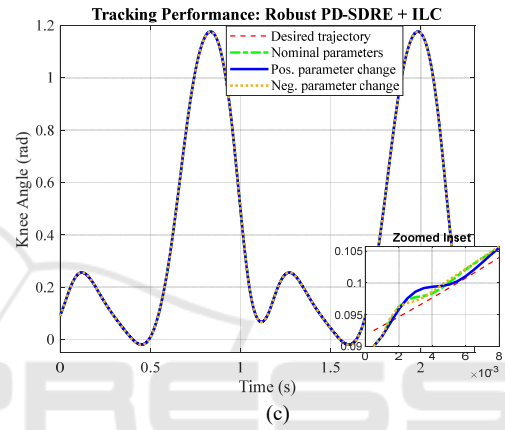
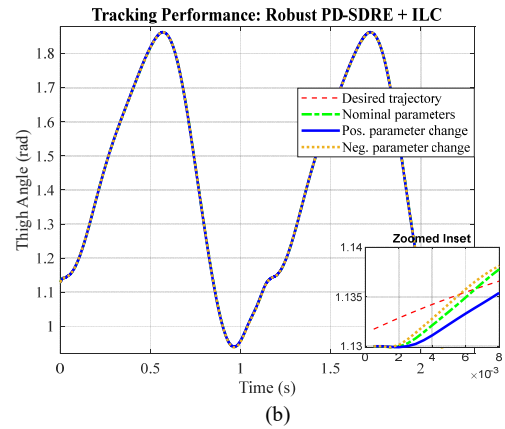
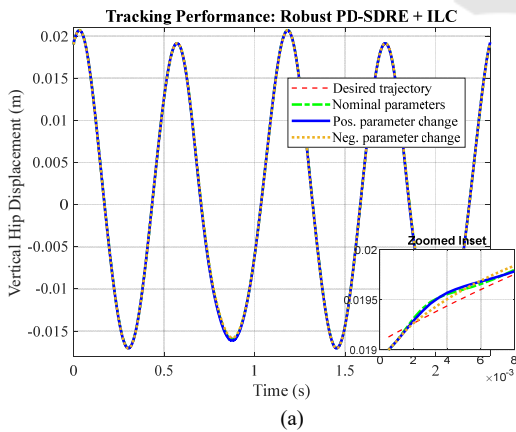


Figure 4: Tracking performance in nominal mode and $\pm 30\%$ parametric change, considering saturation bounds: a) Hip displacement, b) Thigh angle, c) Knee angle.

Figure 5 shows the control signals. Evidently, a peak occurs at the start of the motion, which is due to the difference between the initial state values and the starting points of the desired trajectories. The good performance of the proposed controller is demonstrated also by the fact that the control signals always remain within saturation limits. Furthermore, the amplitude of the control signals, when we change parameters, remains almost identical, indicating the reliability of the proposed controller.

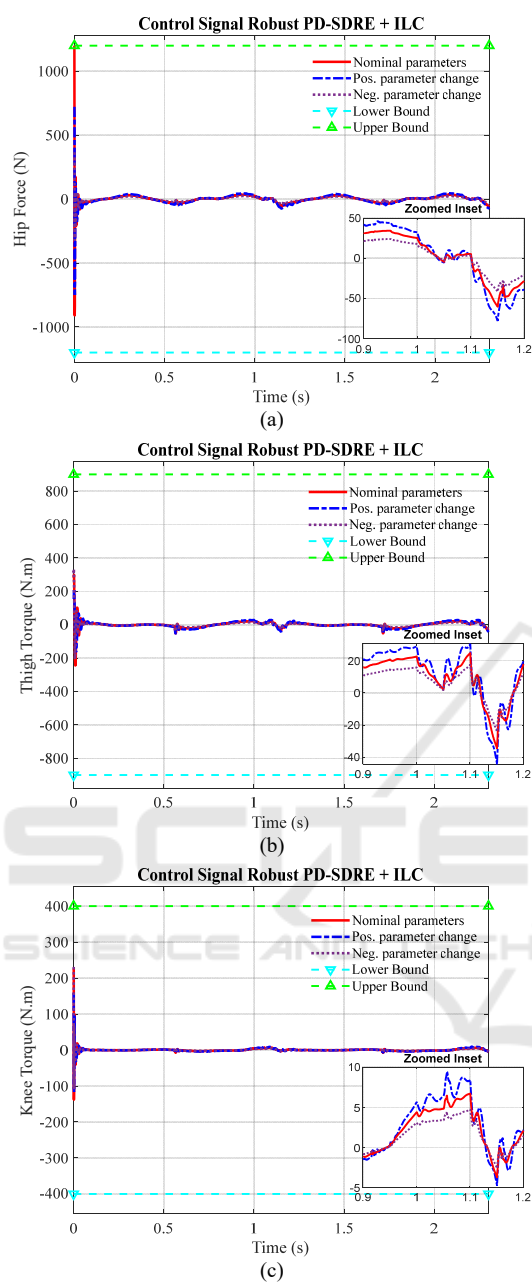


Figure 5: Control signals in nominal mode and $\pm 30\%$ parametric change with saturation bounds a) Hip force, b) Thigh torque, c) Knee torque.

Finally, we also apply a $\pm 30\%$ change to each of the eight parameters P_i individually, modifying only one parameter at a time, with ILC set to five iterations. Despite the change, we again observe good performance, that is, relatively low RMSE values for both position and angle tracking, and a relatively low control effort (not shown, for space reasons).

5 CONCLUSIONS

In this paper, we present a novel control strategy for active prosthetic legs. Our proposed approach, which combines a PD-SDRE controller with ILC and robust SMC, considerably reduced biomechanical energy consumption and improved tracking performance compared to existing approaches. The integration of robust SMC aimed at managing disturbances, to ensure that the system remains resilient under varying conditions, as indicated by our various scenarios of parametric change, while the integration of ILC further improved the control strategy. Our results clearly advance the field of prosthesis control. Despite these promising results, the proposed control strategy has a limitation that should be addressed in future studies. Specifically, the SDRE controller requires full state information, which may not always be directly available in real-world applications. Obtaining all necessary state variables typically demands a large number of sensors, while reducing sensor count remains a significant challenge in robotic leg design. To overcome this issue, future work will focus on the design and integration of a nonlinear state estimator to reduce sensor dependency and further enhance the performance of the proposed control framework. An initial investigation into estimator development has already been reported in our recent study (Bavarsad and August, 2025). In addition, practical implementation of the three-layer controller on a real active prosthetic leg is planned, with experimental validation under various gait conditions to assess real-world applicability and robustness. This promises to bring significant improvements in prosthetics.

REFERENCES

- Ahn, H. S., Chen, Y., & Moore, K. L. (2007). Iterative learning control: Brief survey and categorization. *IEEE Transactions on Systems, Man, and Cybernetics, Part C (Applications and Reviews)*, 37(6), 1099-1121.
- Azimi, V., Simon, D., & Richter, H. (2015, October). Stable robust adaptive impedance control of a prosthetic leg. In *Dynamic Systems and Control Conference* (Vol. 57243, p. V001T09A003). American Society of Mechanical Engineers.
- Bavarsad, A., August, E., (2025). Nonlinear Estimator Based Iterative Learning PD-SDRE Control for Active Transfemoral Prosthetic Legs. The 13th IFAC Symposium on Nonlinear Control Systems (NOLCOS). Reykjavik, Iceland.
- Bavarsad, A., Fakharian, A., & Menhaj, M. B. (2020). Optimal sliding mode controller for an active

- transfemoral prosthesis using state-dependent riccati equation approach. *Arabian Journal for Science and Engineering*, 45(8), 6559-6572.
- Bavarsad, A., Fakharian, A., & Menhaj, M. B. (2021). A nonlinear robust optimal controller for an active transfemoral prosthesis: an estimator-based state-dependent riccati equation approach. *Proceedings of the Institution of Mechanical Engineers, Part I: Journal of Systems and Control Engineering*, 235(3), 313-329.
- Bukowski, E. L. (2006). Atlas of amputations and limb deficiencies: Surgical, prosthetic, and rehabilitation principles, ed 3. *Physical Therapy*, 86(4), 595-596.
- Camargo, J., Bhakta, K., Herrin, K., & Young, A. (2023). Biomechanical evaluation of stair ambulation using impedance control on an active prosthesis. *Journal of Biomechanical Engineering*, 145(2), 021007.
- Chin, T., Sawamura, S., Shiba, R., Oyabu, H., Nagakura, Y., & Nakagawa, A. (2005). Energy expenditure during walking in amputees after disarticulation of the hip: a microprocessor-controlled swing-phase control knee versus a mechanical-controlled stance-phase control knee. *The Journal of Bone & Joint Surgery British Volume*, 87(1), 117-119.
- Çimen, T. (2008). State-dependent Riccati equation (SDRE) control: a survey. *IFAC Proceedings Volumes*, 41(2), 3761-3775.
- Kashiri, N., Abate, A., Abram, S. J., Albu-Schaffer, A., Clary, P. J., Daley, M., ... & Tsagarakis, N. (2018). An overview on principles for energy efficient robot locomotion. *Frontiers in Robotics and AI*, 5, 129.
- Kaufman, K. R., Levine, J. A., Brey, R. H., McCrady, S. K., Padgett, D. J., & Joyner, M. J. (2008). Energy expenditure and activity of transfemoral amputees using mechanical and microprocessor-controlled prosthetic knees. *Archives of physical medicine and rehabilitation*, 89(7), 1380-1385.
- Kibria, Z., & Commuri, S. (2024, June). Intelligent Control of Prosthetic Leg for Gait Symmetry. In *2024 International Symposium on Medical Robotics (ISMR)* (pp. 1-8). IEEE.
- Ma, X., Zhang, X., & Xu, J. (2024). Robotic leg prosthesis: A survey from dynamic model to adaptive control for gait coordination. *IEEE Transactions on Neural Systems and Rehabilitation Engineering*, 32, 607-624.
- Martini, E., Cesini, I., D'Abbraccio, J., Arnetoli, G., Doronzio, S., Giffone, A., ... & Crea, S. (2020). Increased symmetry of lower-limb amputees walking with concurrent bilateral vibrotactile feedback. *IEEE Transactions on Neural Systems and Rehabilitation Engineering*, 29, 74-84.
- McDonald, C. L., Westcott-McCoy, S., Weaver, M. R., Haagsma, J., & Kartin, D. (2021). Global prevalence of traumatic non-fatal limb amputation. *Prosthetics and orthotics international*, 45(2), 105-114.
- Memon, F., & Shao, C. (2021). Data-driven optimal PID type ILC for a class of nonlinear batch process. *International Journal of Systems Science*, 52(2), 263-276.
- Müßig, J. A., Brauner, T., Kröger, I., Varady, P. A., Brand, A., Klöpfer-Krämer, I., ... & Augat, P. (2019). Relation between the amount of daily activity and gait quality in transfemoral amputees. *International Journal of Rehabilitation Research*, 42(2), 139-144.
- Nekoo, S. R. (2019). Tutorial and review on the state-dependent Riccati equation. *Journal of Applied Nonlinear Dynamics*, 8(2), 109-166.
- Nekoo, S. R., Acosta, J. A., Heredia, G., & Ollero, A. (2022). A PD-type state-dependent Riccati equation with iterative Learning Augmentation for Mechanical systems. *IEEE/CAA Journal of Automatica Sinica*, 9(8), 1499-1511.
- Orendurff, M. S., Segal, A. D., Klute, G. K., & McDowell, M. L. (2006). Gait efficiency using the C-Leg. *Journal of rehabilitation research and development*, 43(2), 239.
- Richter, H., Simon, D., Smith, W. A., & Samorezov, S. (2015). Dynamic modeling, parameter estimation and control of a leg prosthesis test robot. *Applied Mathematical Modelling*, 39(2), 559-573.
- Saat, S., Ahmad, M. A., & Ghazali, M. R. International Journal of Cognitive Computing in Engineering.
- Shen, D. (2018). Iterative learning control with incomplete information: A survey. *IEEE/CAA Journal of Automatica Sinica*, 5(5), 885-901.
- Slotine, J. J. E., & Li, W. (1991). *Applied nonlinear control* (Vol. 199, No. 1, p. 705). Englewood Cliffs, NJ: Prentice hall.
- Ziegler-Graham, K., MacKenzie, E. J., Ephraim, P. L., Trivison, T. G., & Brookmeyer, R. (2008). Estimating the prevalence of limb loss in the United States: 2005 to 2050. *Archives of physical medicine and rehabilitation*, 89(3), 422-429.